LU TP 15-37
October 2015

Drell-Yan phenomenology in the color dipole picture revisited

Eduardo Basso,[1,2,*] Victor P. Goncalves,[2,3,†] Jan Nemchik,[4,5,‡] Roman Pasechnik,[2,§] and Michal Šumbera[6,¶]

[1] *Instituto de Física, Universidade Federal do Rio de Janeiro, Caixa Postal 68528, Rio de Janeiro, RJ 21941-972, Brazil*
[2] *Department of Astronomy and Theoretical Physics, Lund University, SE-223 62 Lund, Sweden*
[3] *High and Medium Energy Group, Instituto de Física e Matemática, Universidade Federal de Pelotas, Pelotas, RS, 96010-900, Brazil*
[4] *Czech Technical University in Prague, FNSPE, Břehová 7, 11519 Prague, Czech Republic*
[5] *Institute of Experimental Physics SAS, Watsonova 47, 04001 Košice, Slovakia*
[6] *Nuclear Physics Institute ASCR, 25068 Řež, Czech Republic*

An extensive phenomenological study of the Drell-Yan (DY) process in pp collisions at various energies is performed in the color dipole framework. Besides previously studied γ^* production we have also included the Z^0 contribution relevant at large dilepton invariant masses. We investigate the DY cross section differential in invariant mass, rapidity and transverse momentum of the dilepton pair in pp collisions at RHIC and LHC. We consider three different phenomenological models for the dipole cross section and found a reasonable agreement with the available data. As a further test of the color dipole formalism, we also study the correlation function in azimuthal angle between the dilepton pair and a forward pion $\Delta\phi$ for different energies, dilepton rapidites and invariant masses. The characteristic double-peak structure of the correlation function around $\Delta\phi \simeq \pi$ found for very forward pions and low-mass dilepton pairs is sensitive to the saturation effects and can be tested by future DY measurements in pp collisions.

I. INTRODUCTION

The study of Drell-Yan (DY) processes at the LHC energies provide an important test of the Standard Model (SM) as well as can provide an additional information about New Physics beyond the SM. In particular, the DY process in $pp/pA/AA$ collisions at the LHC is an excellent tool for the investigations of strong interaction dynamics in an extended kinematical range of energies and rapidities (for a recent review see, e.g. Ref. [1]). For example, the recent measurements of the gauge boson production cross section by LHCb experiment [2] at forward rapidities have a sensitivity to x values down to 1.7×10^{-4} at the scale $Q^2 \sim M^2$ (M is the invariant mass of the dilepton) probing the parton distribution functions (PDFs) and soft QCD dynamics in a kinematical range different from that studied by HERA.

During the last two decades several approaches have been proposed to improve the fixed-order QCD perturbation theory description of the DY process which is not reliable when two or more different hard scales are present (see e.g. Refs. [3–13]). A well-known example is the description of the transverse momentum p_T distribution of the dilepton. In the low-p_T region, $p_T \ll M$, there are two powers of $\ln(M^2/p_T^2) \gg 1$ for each additional power of the strong coupling α_s, and the DY p_T distribution calculated in fixed-order QCD perturbation theory is not reliable. Only after resummation of the large terms $\propto \alpha_s^n \ln^{2n+1}(M^2/p_T^2)$ the predictions become consistent with the data. Another example is in the case of the high energies $s \gg M^2$ when potentially large terms $\propto \alpha_s^n \ln^n(s/M^2)$ should also be resummed. In this case, the standard collinear factorisation approach should be generalized by taking into account the transverse momentum evolution of the incoming partons and QCD nonlinear effects.

One of the phenomenological approaches which effectively takes into account the higher-order QCD corrections is the color dipole formalism [14]. At high energies, color dipoles with a definite transverse separation are eigenstates of

*Electronic address: eduardo.basso@thep.lu.se
†Electronic address: victorpbg@thep.lu.se
‡Electronic address: nemcik@saske.sk
§Electronic address: roman.pasechnik@thep.lu.se
¶Electronic address: sumbera@ujf.cas.cz

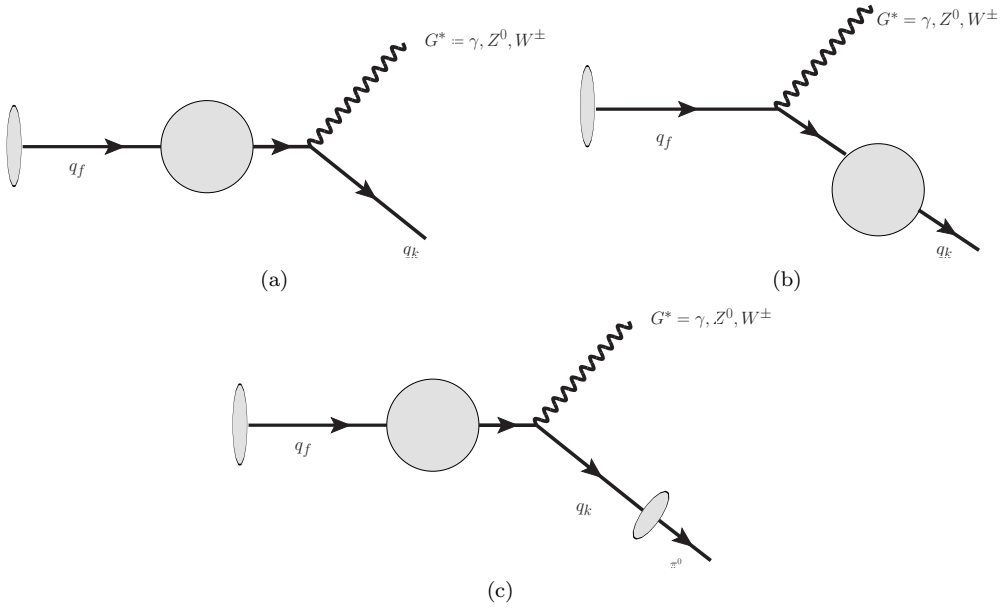

FIG. 1: Diagrams (a) and (b) represent the process of a gauge boson radiation by a quark (antiquark) of flavour f either after or before the interaction with the target color field (denoted by a shaded circle), respectively. For the considered γ, Z^0 radiation $q_k = q_f$. Diagram (c) represents the gauge boson-pion production in the color dipole picture.

interaction. The main ingredient of this formalism is the dipole-target scattering cross section which is universal and process-independent and thus can be determined phenomenologically, for example, from the Deep Inelastic Scattering (DIS) data [15]. In particular, it provides a unified description of inclusive and diffractive observables in *ep* scattering processes as well as other processes in hadron-hadron collisions such as DY, prompt photon and heavy quark production etc [14, 16–21]. Although cross sections are Lorentz invariant, the partonic interpretation of the corresponding processes depends on the reference frame [17]. In particular, in the framework of conventional parton model the DY process is typically considered as due to parton annihilation in the center-of-mass frame description. In the target rest frame the same process can be viewed as a bremsstrahlung of γ/Z in the dipole picture as illustrated in Figs. 1 (a) and (b). In the latter case, the radiation occurs both after and before the quark scatters off the target and the corresponding amplitudes interfere. In the high-energy limit, the projectile quark probes dense gluonic field in the target such that nonlinear effects due to multiple scatterings become important and should be taken into account.

The DY process mediated by virtual photon has been studied within the dipole framework in the literature by several authors (see e.g. Refs. [22–24]). In particular, in Ref. [23] it has been demonstrated that the dipole model provides as precise prediction for the DY cross section as the NLO collinear factorisation framework providing a solid foundation for the current more extensive study. The inclusive gauge bosons production has been previously analysed by some of the authors in Ref. [25] where predictions for the total cross sections and rapidity distributions were found to be in a good agreement with the recent LHC data. In the diffractive channel, the DY and electroweak gauge bosons production has been studied in the dipole framework in Ref. [26].

The goal of the current work is the following. First, we update and improve previous studies presenting predictions for the transverse momentum, invariant mass and rapidity distributions for the DY production at RHIC and LHC energies and compare them with available data. Second, we present a detailed analysis of the azimuthal correlation between the DY pair and a forward pion (see Fig. 1(c)) taking into account Z^0 boson contribution in addition to virtual photon. Similar correlations in dihadron, real photon-hadron and dilepton-hadron channels have been previously in Refs. [27–30]. In variance from dihadron channel, the dilepton-hadron correlations can serve as an efficient probe of the initial state effects since the intermediate virtual boson does not interact with the gluons inside the target hadron and therefore the final state interaction effects are not expected. In this paper, for the first time we present results for such an observable for *pp* collisions at RHIC ($\sqrt{s} = 200$ and 500 GeV) and LHC ($\sqrt{s} = 7$ and 14 TeV) at different M. We test three different models for the dipole cross section accounting for saturation effects [31] in order to estimate the underlined theoretical uncertainties.

This paper is organized as follows. In the next Section, we present a brief overview of gauge boson production in the color dipole framework. Moreover, we derive the differential cross section for the dilepton-hadron production in the momentum representation taking into account both virtual photon and Z^0 boson contributions. In Section III, we

present our results for the total cross sections, invariant mass, rapidity and transverse momentum distributions and compare our predictions with the available data at different energies. Predictions for future RHIC and LHC runs are also given. Furthermore, the azimuthal correlation function is evaluated for the DY-pion production in pp collisions at RHIC and LHC for different dilepton invariant masses. Finally, in Section IV, our main conclusions are summarized.

II. INCLUSIVE GAUGE BOSON PRODUCTION IN THE DIPOLE PICTURE

As was mentioned above, in the color dipole picture the DY process is considered as a bremsstrahlung of a virtual gauge boson G^* where $G = \gamma, Z^0, W^\pm$ [17–19] as illustrated in Fig. 1. In the high energy limit, each of the two graphs factorizes into a production vertex for a given gauge boson times a scattering amplitude of a quark off the target. The quark scatters at different impact parameters depending on whether the gauge boson is radiated after or before the scattering. The interference between these scattering amplitudes implies that the squared matrix element for the gauge boson production is expressed in terms of the universal dipole-target cross section $\sigma_{q\bar{q}}(\rho, x)$ with transverse separation between ρ initial and final quark.

A. Inclusive DY cross section

In order to estimate the hadronic cross section for the inclusive DY process $pp \to G^*X$ one has to note that the gauge boson carries away the light-cone momentum fraction x_1 and α from the projectile proton and quark emitting the gauge boson, respectively. Consequently, the momentum fraction of the quark is given by $x_q = x_1/\alpha$. Then the cross section for the inclusive gauge boson production with invariant mass M and transverse momentum p_T is expressed in terms of the quark (antiquark) densities q_f ($\bar{q}_f$) at momentum fraction x_q as follows

$$\frac{d\sigma(pp \to G^*X)}{\mathrm{d}^2p_T d\eta} = J(\eta, p_T)\,\frac{x_1}{x_1+x_2}\sum_f \sum_{\lambda_G=L,T}\int_{x_1}^1 \frac{d\alpha}{\alpha^2}\left[q_f(x_1/\alpha,\mu_F^2)+\bar{q}_f(x_1/\alpha,\mu_F^2)\right]\frac{d\sigma^f_{\lambda_G}(qN\to qG^*X)}{d\ln\alpha d^2p_T} \tag{1}$$

where

$$J(\eta, p_T) \equiv \frac{dx_F}{d\eta} = \frac{2}{\sqrt{s}}\sqrt{M^2+p_T^2}\,\cosh(\eta)\,, \tag{2}$$

is the Jacobian of transformation between Feynman variable $x_F = x_1 - x_2$ and pseudorapidity η of the virtual gauge boson G^*, and $\mu_F^2 = p_T^2 + (1-x_1)M^2$ is the factorization scale in quark PDFs. In practical calculations below we take $\mu_F \simeq M$, for simplicity. We have checked numerically that such a choice of the factorisation scale is a good approximation in the whole kinematical range we are concerned about in this work. The dilepton cross section analysed below is related to the inclusive $G = \gamma$, Z^0 production cross section (1) as follows

$$\frac{d\sigma(pp \to (G^* \to l\bar{l})X)}{d^2p_T dM^2 d\eta} = \mathcal{F}_G(M)\,\frac{d\sigma(pp\to G^*X)}{d^2p_T d\eta}\,, \tag{3}$$

where

$$\mathcal{F}_\gamma(M) = \frac{\alpha_{em}}{3\pi M^2}\,, \qquad \mathcal{F}_Z(M) = \mathrm{Br}(Z^0 \to l\bar{l})\rho_Z(M)\,. \tag{4}$$

Here, the branching ratio $\mathrm{Br}(Z^0 \to l\bar{l}) \simeq 0.101$, and $\rho_Z(M)$ is the invariant mass distribution of the Z^0 boson in the narrow width approximation

$$\rho_Z(M) = \frac{1}{\pi}\,\frac{M\Gamma_Z(M)}{(M^2-m_Z^2)^2+[M\Gamma_Z(M)]^2}\,, \qquad \Gamma_Z(M)/M \ll 1\,, \tag{5}$$

in terms of the on-shell Z^0 boson mass, m_Z, and its generalized total decay width

$$\Gamma_Z(M) = \frac{\alpha_{em}M}{6\sin^2 2\theta_W}\Big(\frac{160}{3}\sin^4\theta_W - 40\sin^2\theta_W + 21\Big)\,, \tag{6}$$

where θ_W is the Weinberg gauge boson mixing angle in the SM, $\sin^2\theta_W \simeq 0.23$, and $\alpha_{em} = e^2/(4\pi) = 1/137$ is the fine structure constant.

The transverse momentum distribution of the gauge boson G^* can be obtained by a generalization of the well-known formulas for the photon bremsstrahlung in Refs. [22, 23]. The corresponding differential cross section for a given incoming quark flavour f reads

$$\frac{d\sigma^f_{T,L}(qN \to qG^*X)}{d\ln\alpha d^2p_T} = \frac{1}{(2\pi)^2}\sum_{\text{quark pol.}}\int d^2\rho_1 d^2\rho_2 \exp[i\mathbf{p}_T\cdot(\boldsymbol{\rho}_1-\boldsymbol{\rho}_2)]\,\Psi^{V-A}_{T,L}(\alpha,\boldsymbol{\rho}_1,m_f)\Psi^{V-A,*}_{T,L}(\alpha,\boldsymbol{\rho}_2,m_f)$$
$$\times\ \frac{1}{2}\left[\sigma_{q\bar{q}}(\alpha\boldsymbol{\rho}_1,x_2)+\sigma_{q\bar{q}}(\alpha\boldsymbol{\rho}_2,x_2)-\sigma_{q\bar{q}}(\alpha|\boldsymbol{\rho}_1-\boldsymbol{\rho}_2|,x_2)\right], \tag{7}$$

where $x_2 = x_1 - x_F$ and $\boldsymbol{\rho}_{1,2}$ are the quark-G transverse separations in the total radiation amplitude and its conjugated, respectively. Assuming that the projectile quark is unpolarized, the vector and axial-vector wave functions in Eq. (7) are not correlated such that we have write

$$\sum_{\text{quark pol.}}\Psi^{V-A}_{T,L}(\alpha,\boldsymbol{\rho}_1,m_f)\Psi^{V-A,*}_{T,L}(\alpha,\boldsymbol{\rho}_2,m_f) =$$
$$= \Psi^{V}_{T,L}(\alpha,\boldsymbol{\rho}_1,m_f)\Psi^{V,*}_{T,L}(\alpha,\boldsymbol{\rho}_2,m_f)+\Psi^{A}_{T,L}(\alpha,\boldsymbol{\rho}_1,m_f)\Psi^{A,*}_{T,L}(\alpha,\boldsymbol{\rho}_2,m_f), \tag{8}$$

where the averaging over the initial and summation over final quark helicities is performed and the quark flavour dependence comes only via projectile quark mass m_f. Different components in Eq. (8) read [26]

$$\Psi^T_V\Psi^{T*}_V = \frac{(\mathcal{C}^G_f)^2(g^G_{v,f})^2}{2\pi^2}\left\{m_f^2\alpha^4\mathrm{K}_0(\tau\rho_1)\,\mathrm{K}_0(\tau\rho_2)+\left[1+(1-\alpha)^2\right]\tau^2\frac{\boldsymbol{\rho}_1\cdot\boldsymbol{\rho}_2}{\rho_1\rho_2}\mathrm{K}_1(\tau\rho_1)\,\mathrm{K}_1(\tau\rho_2)\right\},$$
$$\Psi^L_V\Psi^{L*}_V = \frac{(\mathcal{C}^G_f)^2(g^G_{v,f})^2}{\pi^2}M^2(1-\alpha)^2\,\mathrm{K}_0(\tau\rho_1)\,\mathrm{K}_0(\tau\rho_2),$$
$$\Psi^T_A\Psi^{T*}_A = \frac{(\mathcal{C}^G_f)^2(g^G_{a,f})^2}{2\pi^2}\left\{m_f^2\alpha^2(2-\alpha)^2\mathrm{K}_0(\tau\rho_1)\,\mathrm{K}_0(\tau\rho_2)+\left[1+(1-\alpha)^2\right]\tau^2\frac{\boldsymbol{\rho}_1\cdot\boldsymbol{\rho}_2}{\rho_1\rho_2}\mathrm{K}_1(\tau\rho_1)\,\mathrm{K}_1(\tau\rho_2)\right\},$$
$$\Psi^L_A\Psi^{L*}_A = \frac{(\mathcal{C}^G_f)^2(g^G_{a,f})^2}{\pi^2}\frac{\tau^2}{M^2}\left\{\tau^2\mathrm{K}_0(\tau\rho_1)\,\mathrm{K}_0(\tau\rho_2)+\alpha^2m_f^2\frac{\boldsymbol{\rho}_1\cdot\boldsymbol{\rho}_2}{\rho_1\rho_2}\mathrm{K}_1(\tau\rho_1)\,\mathrm{K}_1(\tau\rho_2)\right\}, \tag{9}$$

where $\tau^2 = (1-\alpha)M^2+\alpha^2m_f^2$, $\mathrm{K}_{0,1}$ denote the modified Bessel functions of the second kind, and the coupling factors $\mathcal{C}^G_f$ are defined as

$$\mathcal{C}^\gamma_f = \sqrt{\alpha_{em}}e_f, \qquad \mathcal{C}^Z_f = \frac{\sqrt{\alpha_{em}}}{\sin 2\theta_W}, \qquad \mathcal{C}^{W^+}_f = \frac{\sqrt{\alpha_{em}}}{2\sqrt{2}\sin\theta_W}V_{f_uf_d}, \qquad \mathcal{C}^{W^-}_f = \frac{\sqrt{\alpha_{em}}}{2\sqrt{2}\sin\theta_W}V_{f_df_u}, \tag{10}$$

with the vectorial coupling at the leading order given by

$$g^Z_{v,f_u} = \frac{1}{2}-\frac{4}{3}\sin^2\theta_W, \qquad g^Z_{v,f_d} = -\frac{1}{2}+\frac{2}{3}\sin^2\theta_W, \qquad g^W_{v,f} = 1, \tag{11}$$

and

$$g^Z_{a,f_u} = \frac{1}{2}, \qquad g^Z_{a,f_d} = -\frac{1}{2}, \qquad g^W_{a,f} = 1 \tag{12}$$

in the axial-vector case. In the above formulas, $f_u = u,c,t$ and $f_d = d,s,b$ are the flavours of up- and down-type quarks, respectively, $V_{f_uf_d}$ is the CKM matrix element corresponding to $f_u \to f_d$ transition, and e_f is the charge of the projectile quark[1]. In the case of projectile photon we have $g_{v,q} = 1$ and $g_{a,q} = 0$. In the present analysis, we restrict ourselves to study of dilepton $l\bar{l}$ productions channels in pp collisions and therefore we consider production of virtual γ and Z^0 bosons only. For this reason, we leave $W^\pm$ production in the $l\bar{\nu}$ channel for future studies. Integrating over the phase space of the final quark, Eqs. (1) and (3) enable us to study the pseudorapidity, transverse momentum and invariant mass distributions for the DY process.

[1] Also, we are focused only on light quark flavours $f = u,d,s$

B. Dilepton-hadron azimuthal correlations

In order to study the azimuthal angle correlation between the DY pair and a hadron in the final state, we should keep an information about the quark which radiates the virtual gauge boson G^*. This analysis can, in principle, be carried out in the impact parameter representation (for more details, see Appendix B in Ref. [22] for the γ^* case), but numerically it is rather cumbersome due to a large number of oscillating Fourier integrals. Alternatively, one derives the corresponding differential cross section directly in momentum representation as was performed for the γ^* case in Refs. [30, 32–34] and then extend it by incorporating Z^0 boson contribution relevant at large dilepton invariant masses. Our basic goal here is to investigate the dilepton-pion correlations accounting for both virtual γ and Z^0 contributions in pp collisions at high energies and their interference in various kinematical domains in rapidity and dilepton invariant mass. The latter can be straightforwardly generalized to the proton-nucleus case.

A generalisation of the results in Refs. [33, 34] is achieved by accounting for both vector and axial contributions in the gauge boson distribution amplitude $q \to q + G^*$ with unpolarised q and G^*. This leads to the differential cross section for the production of a virtual gauge boson G^* and a hadron h (for simplicity, we take $m_f = 0$ for $f = u, d, s$ in what follows)

$$
\begin{aligned}
\frac{d\sigma(pp \to hG^*X)}{dY\, dy_h d^2p_T d^2p_T^h} &= \int_{\frac{x_h}{1-x_1}}^1 \frac{\mathrm{d}z_h}{z_h^2} \sum_f D_{h/f}(z_h,\mu_F^2)\, x_p q_f(x_p,\mu_F)\,(1-z) S_\perp\, F(x_g,k_T^g) \\
&\times \left\{ \frac{(\mathcal{C}_f^G)^2 g_{v,f}^2}{2\pi} \left[\left(1+(1-z)^2\right) \frac{z^2 {k_T^g}^2}{[P_T^2+\epsilon_M^2]\,[(\mathbf{P}_T + z\mathbf{k}_T^g)^2+\epsilon_M^2]} \right.\right. \\
&\qquad \left.\left. - z^2\epsilon_M^2 \left(\frac{1}{P_T^2+\epsilon_M^2} - \frac{1}{(\mathbf{P}_T + z\mathbf{k}_T^g)^2+\epsilon_M^2} \right)^2 \right] \right. \\
&\quad + \frac{(\mathcal{C}_f^G)^2 g_{a,f}^2}{2\pi} \left[\left(1+(1-z)^2\right) \frac{z^2 {k_T^g}^2}{[P_T^2+\epsilon_M^2]\,[(\mathbf{P}_T + z\mathbf{k}_T^g)^2+\epsilon_M^2]} \right. \\
&\qquad \left.\left. - \frac{z^2\epsilon_M^4}{M^2} \left(\frac{1}{P_T^2+\epsilon_M^2} - \frac{1}{(\mathbf{P}_T + z\mathbf{k}_T^g)^2+\epsilon_M^2} \right)^2 \right] \right\}, \qquad (13)
\end{aligned}
$$

where the couplings $\mathcal{C}_f^G$ and $g_{v/a,f}$ are found in Eqs. (10) – (12), $D_{h/f}$ is the fragmentation function of a quark q which has emitted the gauge boson G^* in the produced hadron h, Y and y_h are the rapidities of the gauge boson G^* and the hadron h in the final state, respectively, $\mathbf{p}_T$ and $\mathbf{p}_T^h$ its transverse momenta, z_h is the momentum fraction of the hadron h relative to the quark q it fragments from, $S_\perp$ is the transverse area of the target whose explicit form is not needed for our purposes here. Other kinematics variables are defined as follows

$$
x_1 = \sqrt{\frac{p_T^2+M^2}{s}}\, e^Y\,, \qquad x_h \simeq \frac{p_T^h}{\sqrt{s}}\, e^{y_h}\,, \qquad x_p = x_1 + \frac{x_h}{z_h}\,, \qquad z = \frac{x_1}{x_p}\,, \qquad \epsilon_M^2 = (1-z)M^2\,, \qquad (14)
$$

$$
x_g = x_1\, e^{-2Y} + \frac{x_h}{z_h}\, e^{-2y_h}\,, \qquad \mathbf{k}_T^q = \frac{\mathbf{p}_T^h}{z_h}\,, \qquad \mathbf{k}_T^g = \mathbf{p}_T + \mathbf{k}_T^q\,, \qquad \mathbf{P}_T = (1-z)\mathbf{p}_T - z\mathbf{k}_T^q\,, \qquad (15)
$$

where x_1 and x_h are the gauge boson G and the hadron h momentum fractions taken from the incoming proton, $\mathbf{P}_T$ is the relative transverse momentum between the gauge boson G^* and the quark q, $\mathbf{k}_T^q$ is the transverse momentum of the quark q in the final state, $\mathbf{k}_T^g$ is the transverse momentum of the exchanged gluon[2]. The quantity $F(x_g, k_T^g)$ denotes the unintegrated gluon distribution function (UGDF) describing the multiple interactions of the incoming quark with the target color field, which can be obtained by a Fourier transform of the dipole cross section $\sigma_{q\bar{q}}(\rho)$ (see Ref. [29] for more details).

Integrating equation (13) over the final hadron h momentum, rapidity and relative angle between G^* and h one

[2] Variables z and x_p have the same physical meaning as α and $x_q \equiv x_1/\alpha$ in Eq. (1), respectively, but now they are related to the kinematics variables corresponding the final hadron z_h, y_h and p_T^h, so different notations are reserved for them to avoid confusion.

arrives at the inclusive gauge boson production cross section

$$\begin{aligned}\frac{d\sigma(pp\to G^*X)}{dY d^2p_T} &= \int_{x_1}^1 \frac{dz}{z}\int d^2k_T^g \sum_f x_p q_f(x_p,\mu_F)\, S_\perp\, F(x_g,k_T^g)\\ &\times \left\{\frac{(\mathcal{C}_f^G)^2 g_{v,f}^2}{2\pi}\left[\left(1+(1-z)^2\right)\frac{z^2 {k_T^g}^2}{[p_T^2+\epsilon_M^2]\,[(\mathbf{p}_T-z\mathbf{k}_T^g)^2+\epsilon_M^2]}\right.\right.\\ &\qquad \left.-z^2\epsilon_M^2\left(\frac{1}{p_T^2+\epsilon_M^2}-\frac{1}{(\mathbf{p}_T-z\mathbf{k}_T^g)^2+\epsilon_M^2}\right)^2\right]\\ &+\frac{(\mathcal{C}_f^G)^2 g_{a,f}^2}{2\pi}\left[\left(1+(1-z)^2\right)\frac{z^2 {k_T^g}^2}{[p_T^2+\epsilon_M^2]\,[(\mathbf{p}_T-z\mathbf{k}_T^g)^2+\epsilon_M^2]}\right.\\ &\qquad \left.\left.-\frac{z^2\epsilon_M^4}{M^2}\left(\frac{1}{p_T^2+\epsilon_M^2}-\frac{1}{(\mathbf{p}_T-z\mathbf{k}_T^g)^2+\epsilon_M^2}\right)^2\right]\right\}. \end{aligned} \tag{16}$$

Eqs. (13) and (16) allow us to construct the correlation function $C(\Delta\phi)$, which depends on the azimuthal angle difference $\Delta\phi$ between the trigger and associate particles. Experimentally, this coincidence probability is defined in terms of the yield of the correlated trigger and associated particle pairs $N_{pair}(\Delta\phi)$ and the trigger particle yield N_{trig} as the following ratio: $C(\Delta\phi)=N_{pair}(\Delta\phi)/N_{trig}$. Therefore, azimuthal correlations are investigated through a coincidence probability defined in terms of a trigger particle, which could be either the gauge boson or the hadron. Here we assume the former as trigger particle, so that the correlation function is written as

$$C(\Delta\phi)=\frac{2\pi\int_{p_T,p_T^h>p_T^{\rm cut}} dp_T p_T\, dp_T^h p_T^h\, \frac{d\sigma(pp\to hG^*X)}{dY dy_h d^2p_T d^2p_T^h}}{\int_{p_T>p_T^{\rm cut}} dp_T p_T\, \frac{d\sigma(pp\to G^*X)}{dY d^2p_T}}\,, \tag{17}$$

where $p_T^{\rm cut}$ is the experimental low cut-off on transverse momenta of the resolved G^* (or dilepton) and h, $\Delta\phi$ is the angle between them.

C. Dipole cross section

For the numerical analysis of the DY observables we need to specify a reliable parametrization for the dipole cross section, $\sigma_{q\bar{q}}(\rho,x)$, which represents elastic scattering of a $q\bar{q}$ dipole of transverse separation ρ at Bjorken x off a nucleon [35], thus it contains an information about possible non linear QCD effects in the hadronic wave function (see e.g. Ref. [31]). It is known to vanish quadratically $\sigma_{q\bar{q}}(\rho,x)\propto\rho^2$ as $\rho\to 0$ due to color screening which is the color transparency property [35–37]. It cannot be predicted reliably because of poorly known higher-order perturbative QCD corrections and non-perturbative effects. However, in recent years several groups have constructed a number of viable phenomenological models based on saturation physics and fits to the HERA and RHIC data (see e.g. Refs. [15, 38–49]).

Since our goal is to extend previous DY studies to the kinematical range probed by the massive gauge boson production, where the main contribution comes from the small dipoles, in what follows we will consider two distinct phenomenological models which take into account the DGLAP evolution as well as the saturation effects. The first one is the model proposed in Ref. [45], denoted BGBK hereafter, where the dipole cross section is given by

$$\sigma_{q\bar{q}}(\rho,x)=\sigma_0\left[1-\exp\left(-\frac{\pi^2}{\sigma_0 N_c}\rho^2\alpha_s(\mu^2)xg(x,\mu^2)\right)\right]\,, \tag{18}$$

where $N_c=3$ is the number of colors, $\alpha_s(\mu^2)$ is the strong coupling constant at the scale μ^2 which is related to the dipole size ρ as $\mu^2=C/\rho^2+\mu_0^2$, with C, μ_0 and σ_0 parameters fitted to HERA data. Moreover, in this model, the gluon density evolves according to DGLAP equation [51] accounting for gluons only

$$\frac{\partial xg(x,\mu^2)}{\partial\ln\mu^2}=\frac{\alpha_s(\mu^2)}{2\pi}\int_x^1 {\rm d}z P_{gg}(z)\frac{x}{z}g(\frac{x}{z},\mu^2)\,, \tag{19}$$

where the gluon density at initial scale μ_0^2 is parametrized as

$$xg(x,\mu_0^2)=A_g x^{-\lambda_g}(1-x)^{5.6}\,. \tag{20}$$

The best fit values of the model parameters are the following: $A_g = 1.2$, $\lambda_g = 0.28$, $\mu_0^2 = 0.52$ GeV^2, $C = 0.26$ and $\sigma_0 = 23$ mb. This model was generalized in Ref. [47] in order to take into account the impact parameter dependence of the dipole cross section and to describe exclusive observables at HERA. In this model, denoted as IP-SAT hereafter, the corresponding dipole cross section is given by

$$\sigma_{q\bar{q}}(\rho, x) = 2 \int d^2b \left[1 - \exp\left(-\frac{\pi^2}{2N_c}\rho^2 \alpha_s(\mu^2) x g(x, \mu^2) T_G(\mathbf{b})\right)\right] \tag{21}$$

with the evolution of the gluon distribution given by Eq. (19). The Gaussian impact parameter dependence is given by $T_G(\mathbf{b}) = (1/2\pi B_G)\exp(-b^2/2B_G)$, where B_G is a free parameter extracted from the t-dependence of the exclusive ep data. The parameters of this model were updated in Ref. [48] by fitting to the recent high precision HERA data [50] providing the following values: $A_g = 2.373$, $\lambda_g = 0.052$, $\mu_0^2 = 1.428$ GeV^2, $B_G = 4.0$ GeV^2 and $C = 4.0$.

$\sqrt{s}$ (TeV)	GBW	BGBK	IP-SAT	DATA (nb)
7	0.950	1.208	0.986	0.937 ± 0.037 (ATLAS) 0.974 ± 0.044 (CMS)
8	1.083	1.427	1.183	1.15 ± 0.37 (CMS)
14	1.852	2.797	2.514	–

TABLE I: Comparison between the GBW, BGBK and IP-SAT predictions for the total cross sections for Z^0 boson production at different values of the c.m. energy. The experimental results are from Refs. [52–54]. The cross sections are given in nanobarns.

Finally, for comparison with previous results existing in the literature, we also consider the Golec-Biernat–Wusthoff (GBW) model [15] based upon a simplified saturated form

$$\sigma_{q\bar{q}}(\rho, x) = \sigma_0 \left(1 - e^{-\frac{\rho^2 Q_s^2(x)}{4}}\right) \tag{22}$$

with the saturation scale

$$Q_s^2(x) = Q_0^2 \left(\frac{x_0}{x}\right)^{\lambda}, \tag{23}$$

where the model parameters $Q_0^2 = 1$ GeV^2, $x_0 = 3.04 \times 10^{-4}$ (4.01×10^{-5}), $\lambda = 0.288$ (0.277) and $\sigma_0 = 23.03$ (29) mb were obtained from the fit to the DIS data without (with) the contribution of the charm quark, respectively.

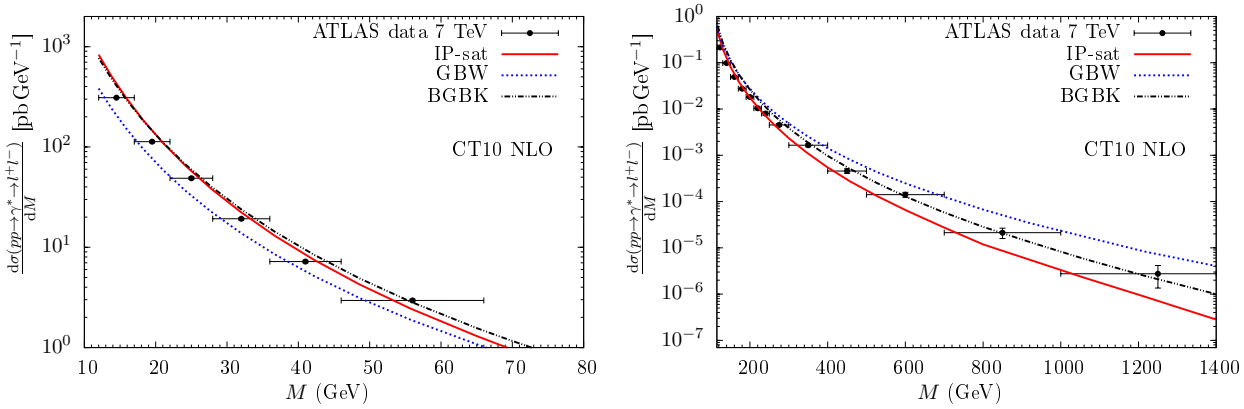

FIG. 2: The DY pair invariant mass distribution of the process $pp \to \gamma^*/Z^0 \to l\bar{l}$ at $\sqrt{s} = 7$ TeV in low (left panel) and high (right panel) invariant mass ranges compared to the data from the ATLAS Collaboration [55, 56] for three different parametrisations of the dipole cross section.

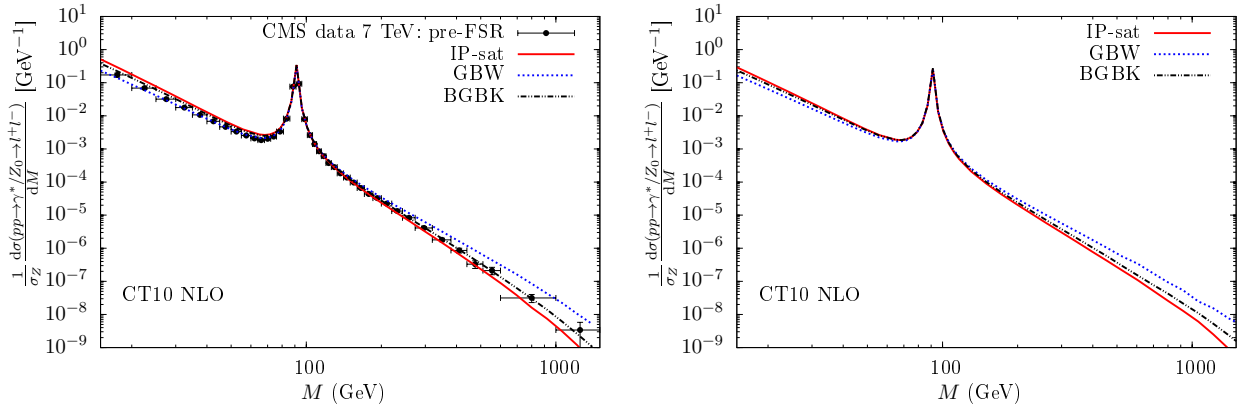

FIG. 3: The DY pair invariant mass distribution of the process $pp \to \gamma^*/Z^0 \to l\bar{l}$ at $\sqrt{s} = 7$ TeV compared to the data from the CMS collaboration [57] for three different parametrisations of the dipole cross section in the left panel. The corresponding predictions are shown for $\sqrt{s} = 14$ TeV in the right panel.

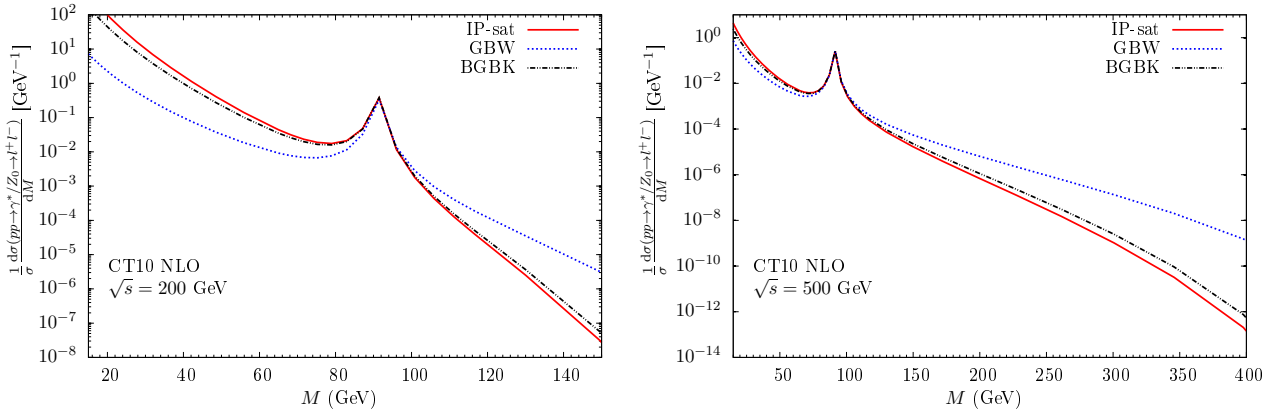

FIG. 4: The DY pair invariant mass distribution of the process $pp \to \gamma^*/Z^0 \to l\bar{l}$ at RHIC Run I ($\sqrt{s} = 200$ GeV) and II ($\sqrt{s} = 500$ GeV) energies for three different parametrisations of the dipole cross section.

III. NUMERICAL RESULTS

In what follows, we present our predictions for the DY pair production in the process $pp \to \gamma^*/Z^0 \to l\bar{l}$ obtained by using the color dipole formalism and the three phenomenological models for the dipole cross section discussed in the previous Section. Following Ref. [15], we take the quark mass values to be $m_u = m_d = m_s = 0.14$ GeV, $m_c = 1.4$ GeV and $m_b = 4.5$ GeV. Moreover, we take the factorization scale μ_F defined above to be equal to the dilepton invariant mass, M, and employ the CT10 NLO parametrization for the projectile quark PDFs [61] (both sea and valences quarks are included).

To start with, in Table I we present our results for the total cross sections for the considered models and different energies. The GBW model gives the total cross section value at 7 TeV smaller than that obtained by using the IP-SAT model correctly treating the region of large transverse momenta (small dipoles). The DY cross section obtained by using the BGBK model turns out to be somewhat higher than the 7 TeV data while the GBW and IP-SAT are well within the error bars while all three models describe 8 TeV data rather well. It is worth to mention that in comparison to Ref. [25] we obtain larger total cross sections for the GBW case since in this study we do not impose any strong relation between $x_{1,2}$ and use the NLO quark PDFs.

Such a fairly good description of the LHC data on the total cross section naturally motivates a more detailed analysis of the DY cross section differential in the dipleton invariant mass, rapidity and transverse momentum. In Fig. 2 we compare our predictions for the invariant mass distributions with the recent ATLAS data in low and high invariant mass ranges. We conclude that the parametrisations of the dipole cross section including the DGLAP evolution via the gluon PDF describe better the DY data, mainly at higher invariant masses. The latter case includes a fairly large

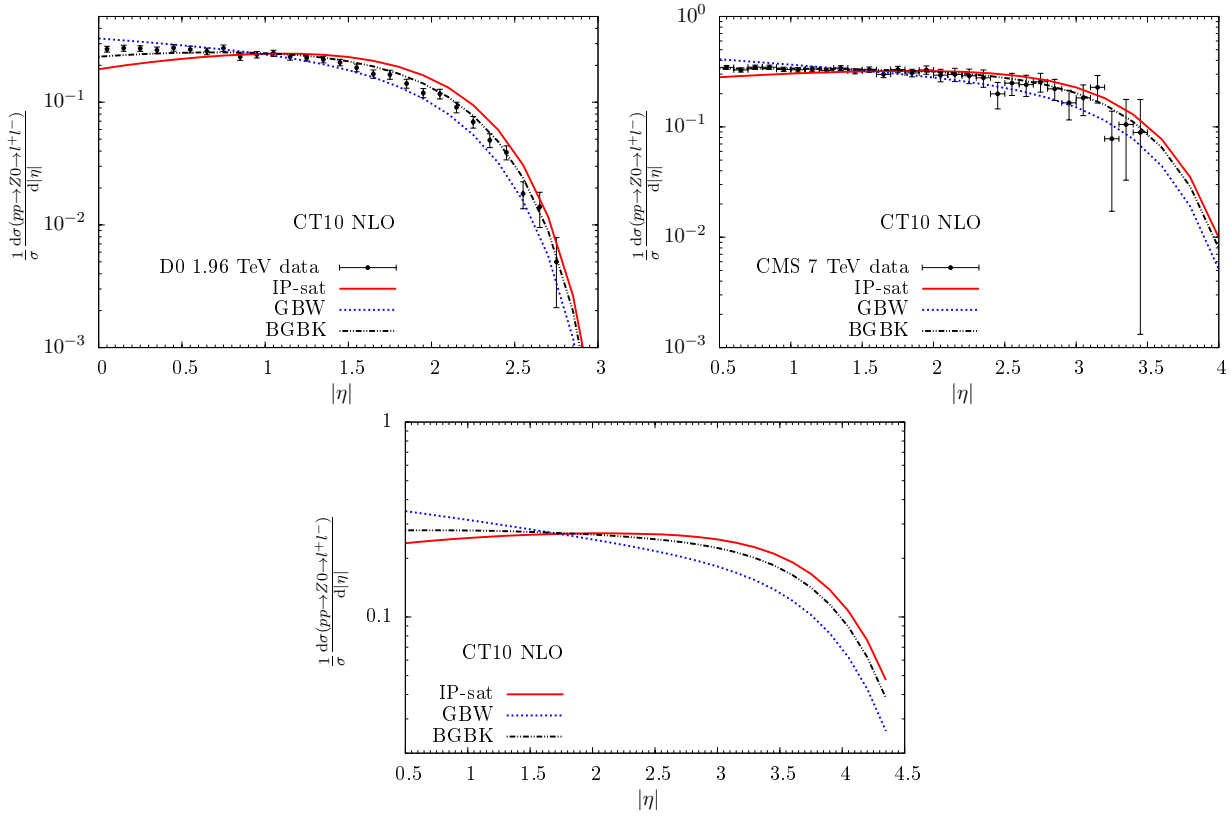

FIG. 5: The Z^0 boson rapidity distribution for different center of mass energies: $\sqrt{s} = 1.96$ TeV (top left panel), 7 TeV (top right panel) and 14 TeV (bottom panel) versus data from the D0 [58] and CMS [59] Collaborations.

Z^0 contribution as well as its interference with γ^* in the considered dilepton channel. It is clearly seen e.g. from a comparison of predictions of the three dipole parametrisations with the CMS data shown in Fig. 3 (left panel). Indeed, the DGLAP evolution, included on both IP-SAT and BGBK models, notably corrects the high mass tail of the distribution, in comparison with the GBW model accounting for no evolution. Our predictions for pp collisions at $\sqrt{s}$ =14 TeV are presented in Fig. 3 (right panel). Considering that a similar measurement can be performed at RHIC, in Fig. 4 we show our results for the dilepton invariant mass distributions corresponding to the c.m. energies of Run I ($\sqrt{s} = 200$ GeV) and II ($\sqrt{s} = 500$ GeV). While the invariant mass distributions corresponding to the IP-SAT and BGBK models are rather close to each other, the GBW prediction noticeably differs from them away from the Z^0 peak, in both low and, especially, high invariant mass ranges.

In Fig. 5 we present our predictions for the Z boson rapidity distribution for different c.m. energies corresponding to Tevatron $\sqrt{s} = 1.96$ TeV (left panel) and LHC Run I $\sqrt{s} = 7$ TeV (center panel). These results show that the IP-SAT and GBW models deviate from data in the central rapidity region while the BGBK predictions come closer to the data in the whole rapidity range. It is worth to emphasize that specifically for the Tevatron energy and for central rapidities, the results are rather sensitive to the behaviour of the dipole cross section at large values of x, which is not under control in the considered formalism. At larger rapidities we obtain a reasonable description of the data though. The future LHC data at $\sqrt{s} = 14$ TeV at large $M > m_Z$ can be used to put even stronger constraints on the dipole model parametrisations (see the right panel in Fig. 5).

We turn now to a discussion of the transverse momentum distributions of the DY pair production cross section. In what follows, we take into account that heavy gauge boson and highly virtual photon production implies that typical dipole separations are small, i.e. $\alpha\rho \sim 1/M^2 \ll \Lambda_{\rm QCD}$. In this limit, the Fourier integral in Eq. (7) can be performed analytically. Taking into account only the leading term in the exponential in the parametrisations for the dipole cross section one has

$$\sigma(\rho, x) \approx \omega(x)\rho^2\,, \qquad \omega(x) = \frac{\pi^2}{2N_c}\,\alpha_s(\mu^2)\,xg(x,\mu^2)\,T_G(\mathbf{b})\,, \tag{24}$$

for the IP-SAT model (a similar analysis can be done for the GBW and BGBK models). The effective dipole cross

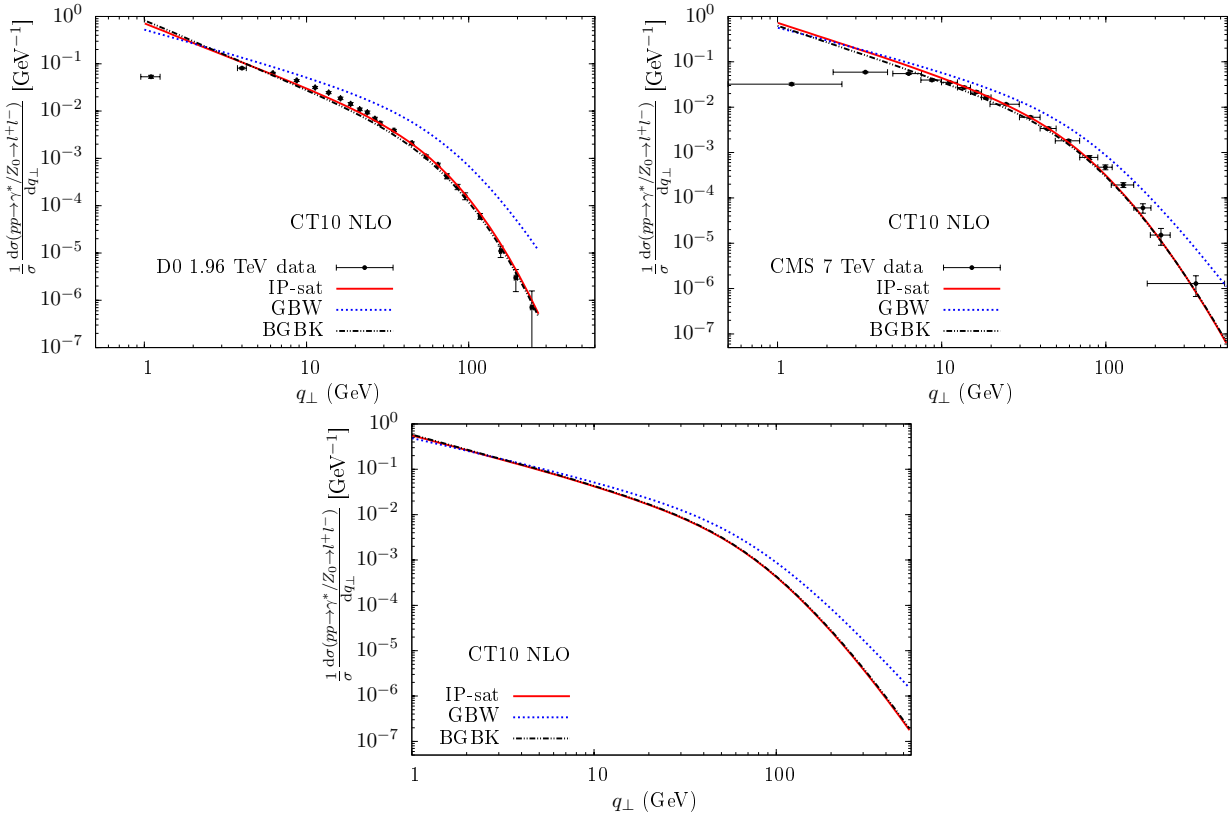

FIG. 6: The transverse momentum distributions of Z^0 bosons in pp collisions at $\sqrt{s} = 1.96$ TeV (top left panel), 7 TeV (top right panel) and 14 TeV (bottom panel) versus data from the D0 [60] and CMS [59] Collaborations.

section in Eq. (7) can thus be written as

$$\sigma_{q\bar{q}}(\alpha\boldsymbol{\rho}_1, x) + \sigma_{q\bar{q}}(\alpha\boldsymbol{\rho}_2, x) - \sigma_{q\bar{q}}(\alpha|\boldsymbol{\rho}_1 - \boldsymbol{\rho}_2|, x) \approx \alpha^2 \boldsymbol{\rho}_1\boldsymbol{\rho}_2\omega\,, \tag{25}$$

so that, taking the ρ dependent part of the gauge boson wave functions in Eq. (9), one ends up with the following two Fourier integrals in the DY cross section (for more details, see Appendix B in Ref. [22])

$$J_1(p_T,\tau) = \int d^2\rho_1 d^2\rho_2\ (\boldsymbol{\rho}_1\cdot\boldsymbol{\rho}_2)\ \mathrm{K}_0\left(\tau\rho_1\right)\ \mathrm{K}_0\left(\tau\rho_2\right)\exp[i\mathbf{p}_T\cdot(\boldsymbol{\rho}_1-\boldsymbol{\rho}_2)] = 16\pi^2\frac{p_T^2}{(\tau^2+p_T^2)^4} \tag{26}$$

$$J_2(p_T,\tau) = \int d^2\rho_1 d^2\rho_2\ \frac{(\boldsymbol{\rho}_1\cdot\boldsymbol{\rho}_2)^2}{\rho_1\rho_2}\ \mathrm{K}_1\left(\tau\rho_1\right)\ \mathrm{K}_1\left(\tau\rho_2\right)\exp[i\mathbf{p}_T\cdot(\boldsymbol{\rho}_1-\boldsymbol{\rho}_2)] = 8\pi^2\frac{\tau^4+p_T^4}{\tau^2(\tau^2+p_T^2)^4}\,. \tag{27}$$

The considered small dipole limit is valid as long as the hard scale is large enough meaning that the dipole coherence length is much larger than the interaction time with the target. The latter condition is certainly fulfilled for the DY-pair transverse momentum distributions at the LHC in a wide range of transverse momenta. One should note, however, that the low dilepton transverse momentum region dominated by larger dipoles is not considered here, as well as realistic cuts on the final lepton momenta that affect the p_T distributions at $p_T \lesssim 10$ GeV are no included in this work. Moreover, at low transverse momenta the contribution of an intrinsic primordial transverse momentum of the projectile quark in the incoming proton wave function and the corresponding Sudakov resummation of double logarithms can be important. We postpone the analysis of these contributions within the dipole formalism for a future investigation.

We present our predictions for the dilepton p_T distribution in Fig. 6 for pp collisions at various energies: $\sqrt{s} = 1.96$ TeV (left panel), 7 TeV (middle panel) and 14 TeV (right panel). As was anticipated, these do not describe the experimental data in the range of low $p_T \lesssim 3$ GeV. On the other hand, at larger p_T the data are well described by the DGLAP evolved dipole models IP-SAT and BGBK, but not GBW. In Fig. 7 we present the corresponding distributions at RHIC energies considering two different ranges of invariant masses. At low invariant masses, where

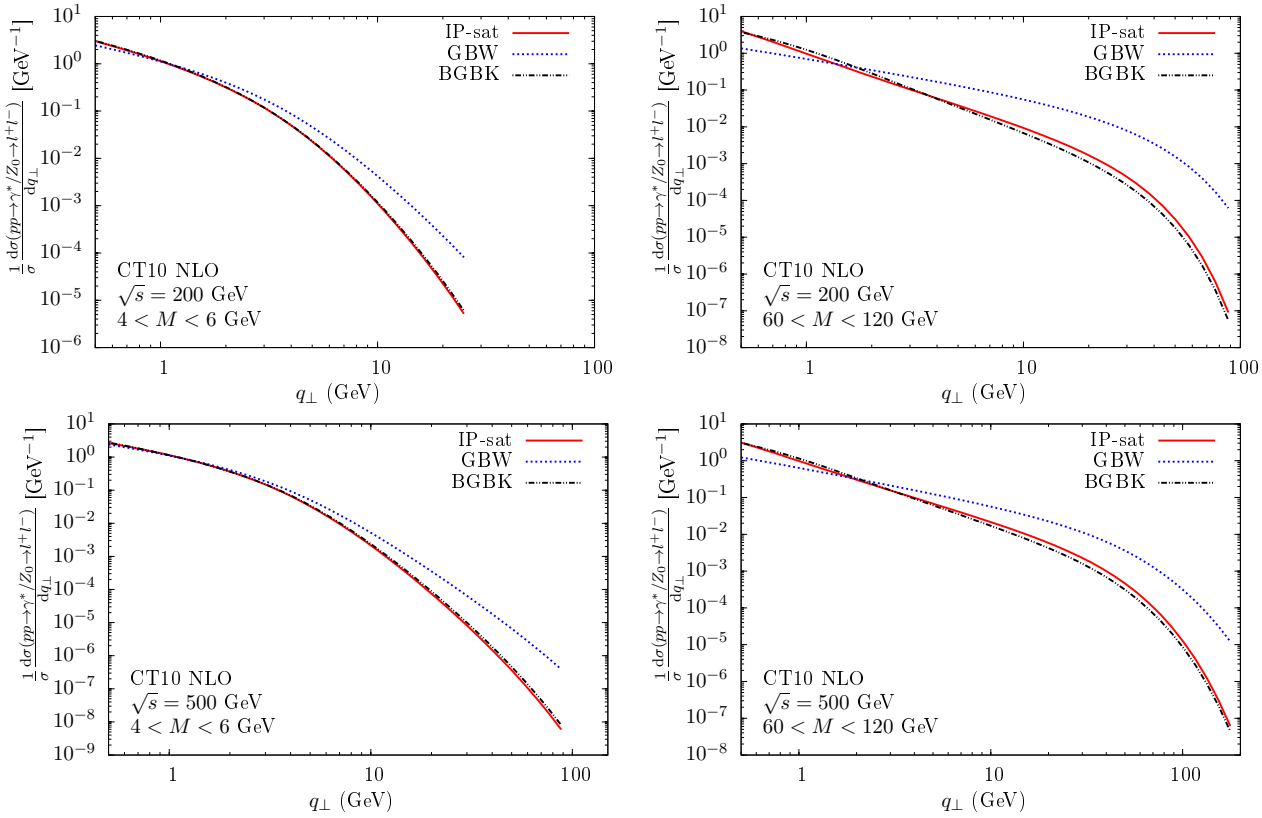

FIG. 7: The transverse momentum distributions for DY production in pp collisions at RHIC ($\sqrt{s} = 200, 500$ TeV) considering two different invariant mass ranges.

the photon channel strongly dominates, the IP-SAT and GBW models give very similar predictions at low p_T, with some minor difference between them at larger transverse momenta. In contrast, at large invariant masses probing the Z peak region, the predictions differ more significantly, and this tendency continues to higher M. In this kinematical range, the DGLAP evolution corrects the tail of the distributions at both low (RHIC) and high (LHC) energies in the same way.

Finally, consider the correlation function $C(\Delta\phi)$ defined in Eq. (17). This observable has been studied in Ref. [28] for the DY+pion production in proton/deuteron-nucleus collisions at RHIC and LHC energies taking into account the saturation effects and considering the virtual photon contribution $\gamma^* \to l\bar{l}$ only. The authors have demonstrated that at variance to the near-side peak ($\Delta\phi = 0$) distribution, which is dominated by the leading jet fragmentation, the away-side peak ($\Delta\phi = \pi$) is dominated by back-to-back jets produced in the hard $2 \to 2$ scattering. Moreover, since low-x gluons in the target dominate and carry a typically large transverse momentum of the order of the saturation scale, the transverse momentum imbalance of the back-to-back jets increases at high energies. So the saturated gluons from the target tend to smear the back-to-back picture and suppress the away-side peak in the $\Delta\phi$ distribution.

Two important results emerge from the analysis performed in Ref. [28]. First, the prediction of a double peak in the correlation function around $\Delta\phi = \pi$, with a dip in $\Delta\phi = \pi$. Second, such a behaviour is not strongly dependent on the large transverse momentum tail of the UGDF used as as input in the calculations. The latter conclusion implies that it is possible to get realistic predictions using the GBW model for the dipole cross section. In this case, numerical issues associated with the Fourier transformation of oscillating functions are not present, and the UGDF can be calculated analytically

$$F(x_g, k_T^g) = \frac{1}{\pi Q_s^2(x_g)}\, e^{-k_T^{g\,2}/Q_s^2(x_g)}\,, \tag{28}$$

with the saturation scale given in Eq. (23). In what follows, we study the correlation function $C(\Delta\phi)$ assuming the GBW model for the UGDF, the CT10 NLO parametrization for the parton distributions and the Kniehl-Kramer-Potter (KKP) fragmentation function $D_{h/f}(z_h, \mu_F^2)$ of a quark to a neutral pion [62]. Moreover, we assume that the

minimum transverse momentum ($p_T^{\rm cut}$) for the gauge boson G and the pion $h = \pi$ in Eq. (17) are the same and equal to 1.5 (3.0) GeV for RHIC (LHC) energies.

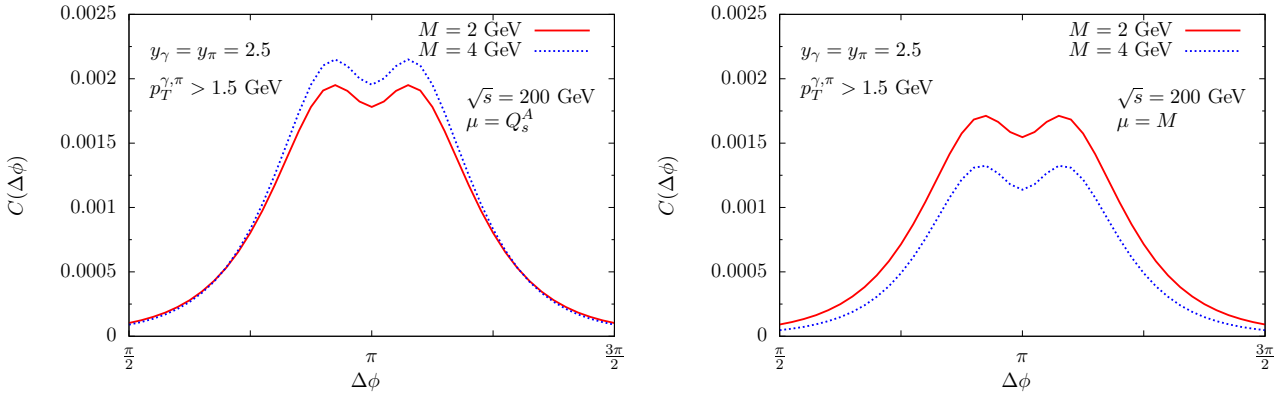

FIG. 8: The correlation function $C(\Delta\phi)$ for the associated DY pair and pion production in dAu collisions at RHIC ($\sqrt{s} = 200$ GeV) assuming that factorization scale is given by the nuclear saturation scale $\mu_F = Q_s^A$ (left panel) or by the dilepton invariant mass $\mu_F = M$ (right panel).

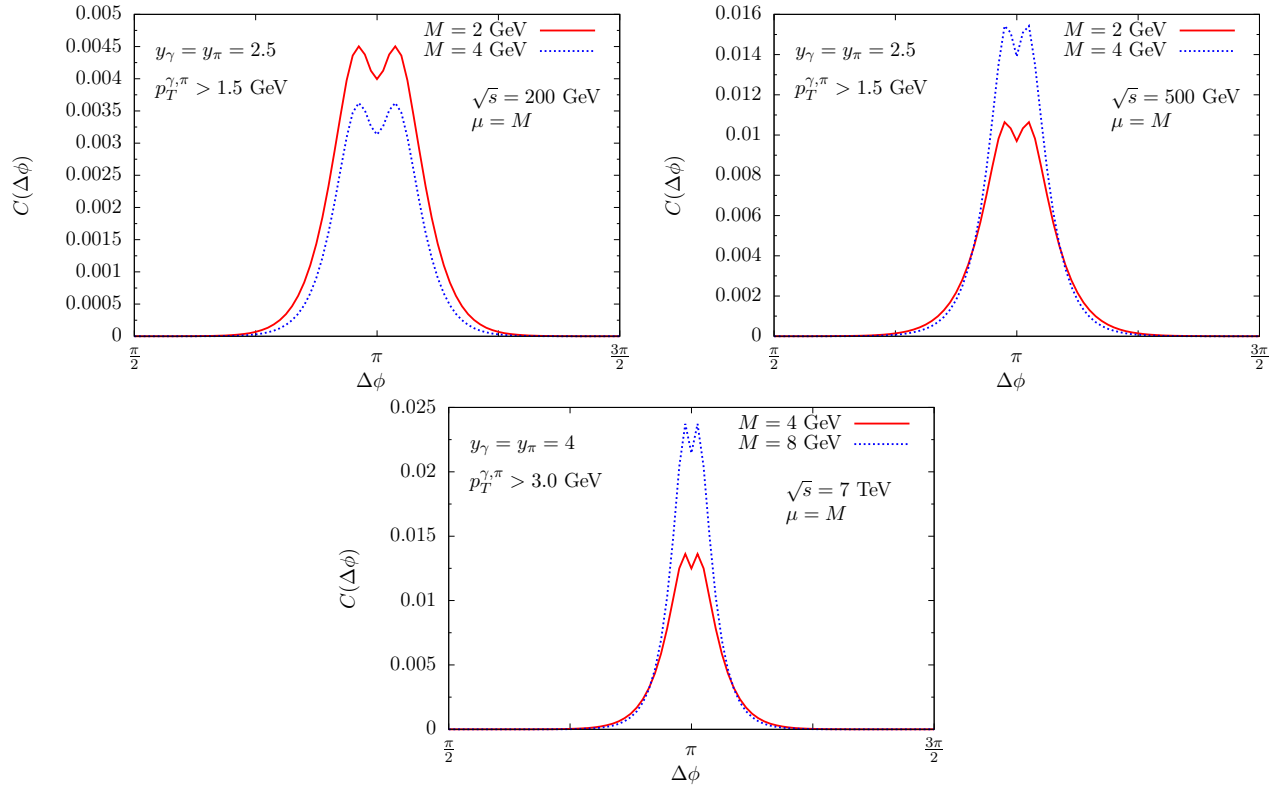

FIG. 9: The correlation function $C(\Delta\phi)$ for the associated DY pair and pion production in pp collisions at RHIC and LHC.

At first, let us compare our results with those presented in Ref. [28] for dAu collisions at RHIC ($\sqrt{s} = 200$ GeV). As in Ref. [28] we take the saturation momentum scale $Q_{s,A}$ for a target nuclei with mass number A as defined by $Q_s^{A\,2}(x) = A^{1/3} c(b)\, Q_s^2(x)$ in terms of the corresponding scale $Q_s(x)$ for the proton target in the GBW parametrisation, where $c(b)$ is the profile function as a function of impact parameter b. Our results for forward particles $y_\gamma = y_\pi = 2.5$ and two different values of the invariant mass M are presented in Fig. 8 (left panel) assuming that the factorization scale of the considering process is determined by the saturation scale, i.e. $\mu_F = Q_s^A$ in Eqs. (13) and (16). As in

Ref. [28], we obtain the double-peak structure in $C(\Delta\phi)$ in the away side, with the magnitude of the peaks increasing with the dilepton invariant mass. The normalisation of the curves turns out to be slightly different from that in Ref. [28], due to the different sets of parton distributions and fragmentation functions used in our calculations, but an overall agreement is rather good.

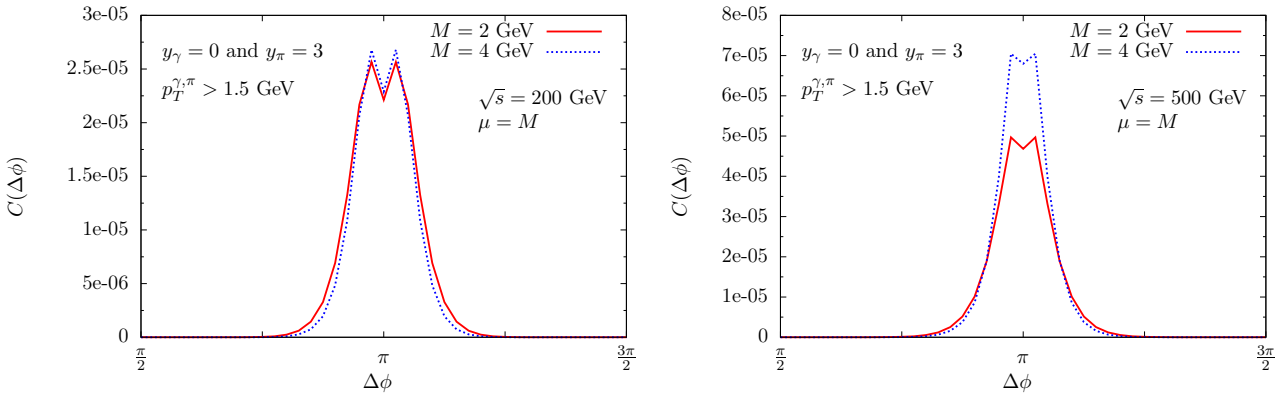

FIG. 10: The correlation function $C(\Delta\phi)$ for the the associated DY pair and pion production in pp collisions at RHIC ($\sqrt{s} = 200, 500$ TeV) for different values of the photon and pion rapidities.

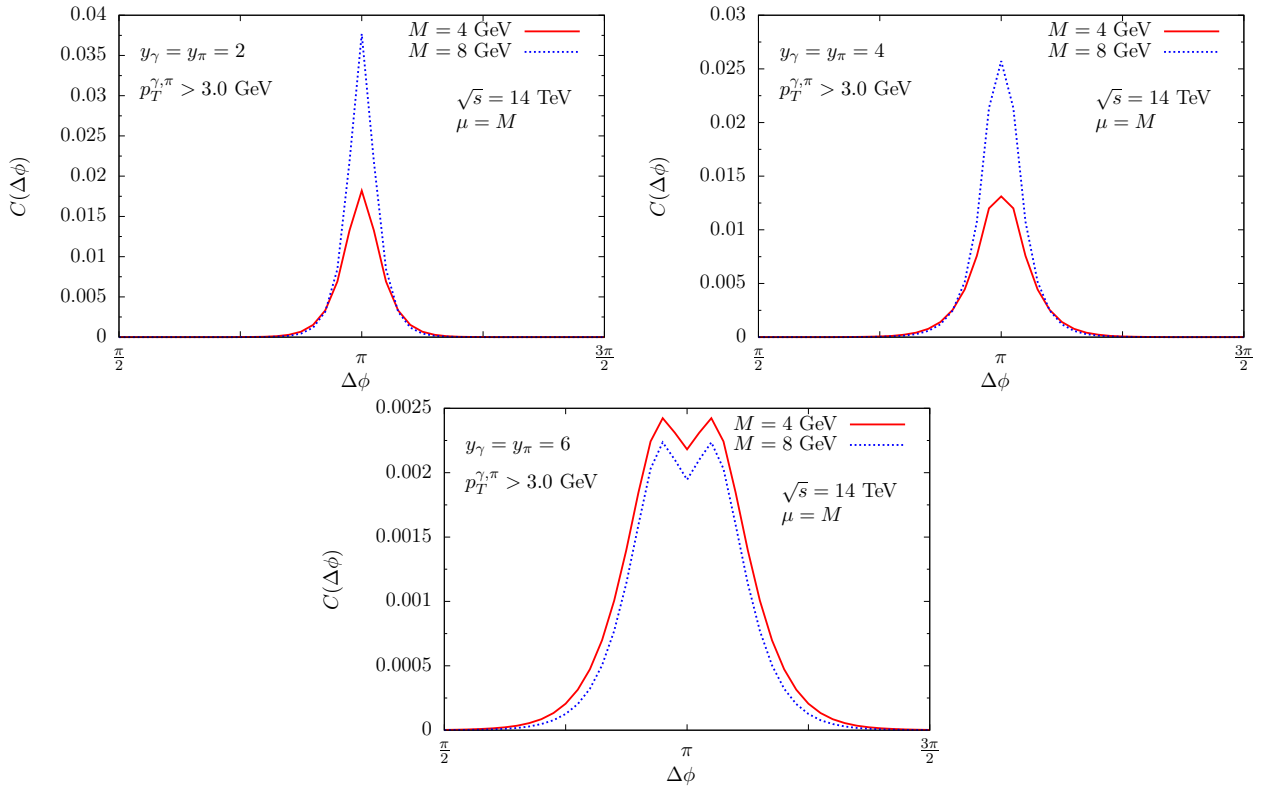

FIG. 11: The correlation function $C(\Delta\phi)$ for the associated DY pair and pion production in pp collisions at LHC ($\sqrt{s} = 14$ TeV) at various values for the gauge boson and pion rapidities.

As at the leading order the choice of the factorisation scale is arbitrary, it can be instructive to analyse the impact of a different scale choice to these results. In Fig. 8 (right panel) we present the results for dAu collisions at RHIC. This choice is motivated by the fact that we would like to extend the formalism used in Ref. [28] for pp collisions and for the kinematical range of large invariant masses where Z^0 must be included. Remarkably, we have observed that

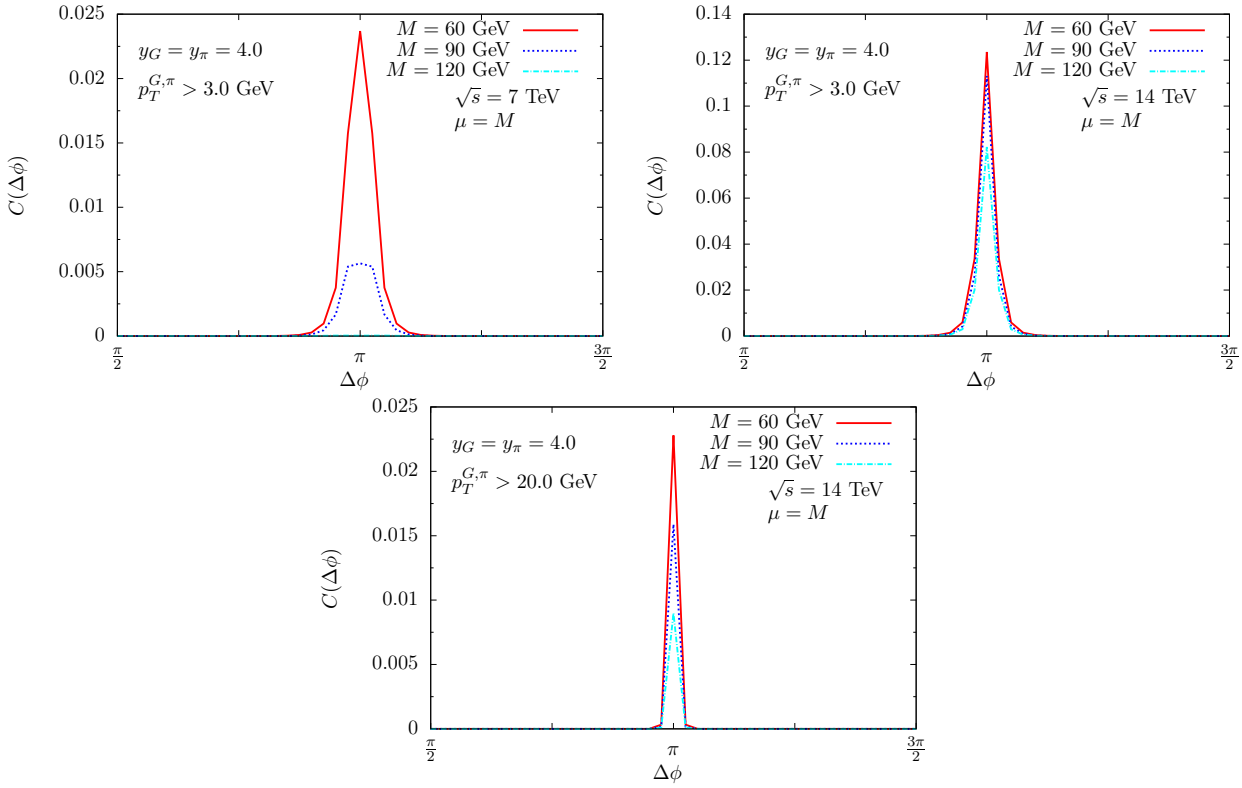

FIG. 12: The correlation function $C(\Delta\phi)$ for the the associated DY pair and pion production in pp collisions at the LHC ($\sqrt{s} = 7, 14$ TeV) for different values of the minimum cut-off $p_T^{\rm cut}$ on the gauge boson and pion transverse momenta.

the double peak structure does also present in the pp case at very forward rapidities and it is not affected by the new choice for the factorization scale, only the invariant mass dependence is modified.

Let us now consider the correlation function in pp collisions. To start with, in Figs. 9 and 11, we show our predictions for the low invariant mass range dominated by the virtual photon $\gamma^* \to l\bar{l}$ channel. In particular, Fig. 9 demonstrates that the double peak structure emerges in pp collisions at both RHIC and LHC energies considering that the photon and the pion are produced at forward rapidities, close to the phase space limit. The double peak structure is also present for different values of the photon (central) and pion (forward) rapidities – the corresponding results at RHIC energies are shown in Fig. 10. It is important to emphasize that the forward-central correlation in such a kinematical configuration can be experimentally studied by the STAR Collaboration in both pp and pA collisions. In Fig. 11 we present the correlation function in pp collisions at $\sqrt{s} = 14$ TeV considering different values for the dilepton pair and pion rapidities. We observe that the double peak structure only arises for the pion at very forward rapidities, where the saturation scale takes a large value of the order of the dilepton invariant mass. Indeed, at large pion rapidities the saturation scale increases and becomes non-negligible compared to the typical transverse momentum of the back-to-back particles which induces a noticeable decorrelation between them. Consequently, these results demonstrate that the study of the rapidity dependence of the correlation function in pp collisions at the LHC Run II can be useful to probe the onset of the saturation effects.

Finally, in Fig. 12 we present our predictions for $C(\Delta\phi)$ for high values of the invariant mass determined by the virtual $Z^0 \to l\bar{l}$ channel and Z^0/γ interference. In the left (middle) panel we present our results for $\sqrt{s} = 7$ (14) TeV assuming that $p_T^{\rm cut} = 3$ GeV. For comparison, in the right panel we also present the results obtained considering $p_T^{\rm cut} = 20$ GeV. In all cases, we obtain a sharp peak for $\Delta\phi \approx \pi$, which is characteristic to the back-to-back kinematics of the final states. This result is expected since at large invariant masses the effect of the intrinsic transverse momentum of the gluon, which is of the order of the saturation scale, is negligible.

IV. SUMMARY

In this paper, we carried out an extensive phenomenological analysis of the inclusive DY $\gamma^*/Z^0 \to l\bar{l}$ process within the color dipole approach. At large dilepton invariant mass the Z^0 contribution becomes relevant. The corresponding predictions for the integrated cross section as well as the dilepton invariant mass and transverse momenta differential distributions have been compared with available data at different energies from Tevatron and LHC. The results were obtained by employing recent IP-SAT and BGBK parametrisations for the dipole cross section accounting for the DGLAP evolution for the gluon density in the target nucleon and a reasonable agreement with the data was found in both low and high invariant mass ranges.

Besides, we have studied correlation function $C(\Delta\phi)$ in azimuthal angle between the produced dilepton and a pion which results by a fragmentation from a projectile quark radiating the virtual gauge boson. The corresponding observable has been studied at various energies in pp collisions in both low and high dilepton invariant mass ranges as well as at different rapidities of final states. We found a characteristic double-peak structure of the correlation function around $\Delta\phi \simeq \pi$ in the case of low dilepton mass and a very forward pion. The considering observable is more exclusive than the ordinary DY process and such a measurement at different energies at RHIC and LHC is therefore capable of setting further even stronger constraints on the UGDF models and, hence, to the dipole model parametrisations offering a possibility for a more direct measurement of the saturation scale.

Acknowledgements

E. B. is supported by CAPES and CNPq (Brazil), contract numbers 2362/13-9 and 150674/2015-5. V. P. G. has been supported by CNPq, CAPES and FAPERGS, Brazil. R. P. is supported by the Swedish Research Council, contract number 621-2013-428. J. N. is partially supported by the grant 13-20841S of the Czech Science Foundation (GAČR), by the Grant MSMT LG13031, by the Slovak Research and Development Agency APVV-0050-11 and by the Slovak Funding Agency, Grant 2/0020/14. M. Š. is supported by the grant LG 13031 of the Ministry of Education of the Czech Republic and by the grant 13-20841S of the Czech Science Foundation (GACR).

[1] J. C. Peng and J. W. Qiu, Prog. Part. Nucl. Phys. **76**, 43 (2014).
[2] R. Aaij *et al.* [LHCb Collaboration] JHEP **06**, 058 (2012); JHEP **01**, 111 (2013); JHEP **02**, 106 (2013).
[3] J. C. Collins, D. E. Soper and G. F. Sterman, Nucl. Phys. B **250**, 199 (1985).
[4] R. Hamberg, W. L. van Neerven and T. Matsuura, Nucl. Phys. B **345**, 331 (1990); Nucl. Phys. B **359**, 343 (1991) [Erratum-ibid. B **644**, 403 (2002)];
W. L. van Neerven and E. B. Zijlstra, Nucl. Phys. B **382**, 11 (1992) [Erratum-ibid. B **680**, 513 (2004)].
[5] J. w. Qiu and G. F. Sterman, Nucl. Phys. B **353**, 105 (1991); Nucl. Phys. B **353**, 137 (1991).
[6] J. w. Qiu and X. f. Zhang, Phys. Rev. Lett. **86**, 2724 (2001);
J. w. Qiu, R. Rodriguez and X. f. Zhang, Phys. Lett. B **506**, 254 (2001);
E. L. Berger, J. w. Qiu and X. f. Zhang, Phys. Rev. D **65**, 034006 (2002);
G. I. Fai, J. w. Qiu and X. f. Zhang, Phys. Lett. B **567**, 243 (2003).
[7] G. Watt, A. D. Martin and M. G. Ryskin, Phys. Rev. D **70**, 014012 (2004) [Erratum-ibid. D **70**, 079902 (2004)].
[8] S. P. Baranov, A. V. Lipatov and N. P. Zotov, Phys. Rev. D **78**, 014025 (2008); J. Phys. G **36**, 125008 (2009).
[9] M. Deak and F. Schwennsen, JHEP **0809**, 035 (2008).
[10] F. Hautmann, M. Hentschinski and H. Jung, Nucl. Phys. B **865**, 54 (2012).
[11] S. Marzani and R. D. Ball, Nucl. Phys. B **814**, 246 (2009).
[12] S. Catani and M. Grazzini, Phys. Rev. Lett. **98**, 222002 (2007);
S. Catani, L. Cieri, G. Ferrera, D. de Florian and M. Grazzini, Phys. Rev. Lett. **103**, 082001 (2009).
[13] M. Bonvini, S. Forte and G. Ridolfi, Nucl. Phys. B **847**, 93 (2011).
[14] N. N. Nikolaev, B. G. Zakharov, Z. Phys. C **64**, 631 (1994).
[15] K. J. Golec-Biernat, M. Wusthoff, Phys. Rev. D **59**, 014017 (1998).
[16] N. N. Nikolaev and B. G. Zakharov, J. Exp. Theor. Phys. **78**, 598 (1994) [Zh. Eksp. Teor. Fiz. **105**, 1117 (1994)]; Z. Phys. C **64**, 631 (1994).
[17] B. Z. Kopeliovich, in *Proceedings of the international workshop XXIII on Gross Properties of Nuclei and Nuclear Excitations, Hirschegg, Austria, 1995*, edited by H. Feldmeyer and W. Nörenberg (Gesellschaft Schwerionenforschung, Darmstadt, 1995), p. 385.
[18] S. J. Brodsky, A. Hebecker and E. Quack, Phys. Rev. D **55**, 2584 (1997).
[19] B. Z. Kopeliovich, A. Schafer, and A. V. Tarasov, Phys. Rev. C **59**, 1609 (1999).
[20] B. Z. Kopeliovich, J. Raufeisen, and A. V. Tarasov, Phys. Lett. B **503**, 91 (2001).

[21] N. N. Nikolaev, G. Piller and B. G. Zakharov, Z. Phys. A **354**, 99 (1996);
B. Z. Kopeliovich and A. V. Tarasov, Nucl. Phys. A **710**, 180 (2002).
[22] B. Z. Kopeliovich, J. Raufeisen, A. V. Tarasov and M. B. Johnson, Phys. Rev. C **67**, 014903 (2003).
[23] J. Raufeisen, J. -C. Peng and G. C. Nayak, Phys. Rev. D **66**, 034024 (2002);
M. B. Johnson, B. Z. Kopeliovich, M. J. Leitch, P. L. McGaughey, J. M. Moss, I. K. Potashnikova and I. Schmidt, Phys. Rev. C **75**, 035206 (2007);
M. B. Johnson, B. Z. Kopeliovich and I. Schmidt, Phys. Rev. C **75**, 064905 (2007).
[24] M. A. Betemps, M. B. Gay Ducati and M. V. T. Machado, Phys. Rev. D **66**, 014018 (2002);
M. A. Betemps, M. B. G. Ducati, M. V. T. Machado and J. Raufeisen, Phys. Rev. D **67**, 114008 (2003);
M. A. Betemps and M. B. Gay Ducati, Phys. Rev. D **70**, 116005 (2004); Phys. Lett. B **636**, 46 (2006);
M. A. Betemps, M. B. Gay Ducati and E. G. de Oliveira, Phys. Rev. D **74**, 094010 (2006);
M. B. Gay Ducati and E. G. de Oliveira, Phys. Rev. D **81**, 054015 (2010);
M. B. G. Ducati, M. T. Griep and M. V. T. Machado, Phys. Rev. D **89**, no. 3, 034022 (2014).
[25] E. A. F. Basso, V. P. Goncalves and M. Rangel, Phys. Rev. D **90**, no. 9, 094025 (2014).
[26] R. S. Pasechnik, B. Z. Kopeliovich, and I. K. Potashnikova, Phys. Rev. D **86**, 114039 (2012).
[27] C. Marquet, Nucl. Phys. A **796**, 41 (2007); J. L. Albacete and C. Marquet, Phys. Rev. Lett. **105**, 162301 (2010).
[28] A. Stasto, B. W. Xiao and F. Yuan, Phys. Lett. B **716**, 430 (2012).
[29] A. Stasto, B-W Xiao and D. Zaslavsky, Phys. Rev.D **86**, 014009 (2012).
[30] J. Jalilian-Marian and A. H. Rezaeian, Phys. Rev. D **86**, 034016 (2012);
A. H. Rezaeian, Phys. Rev. D **86**, 094016 (2012).
[31] F. Gelis, E. Iancu, J. Jalilian-Marian and R. Venugopalan, Ann. Rev. Nucl. Part. Sci. **60**, 463 (2010);
E. Iancu and R. Venugopalan, arXiv:hep-ph/0303204;
H. Weigert, Prog. Part. Nucl. Phys. **55**, 461 (2005);
J. Jalilian-Marian and Y. V. Kovchegov, Prog. Part. Nucl. Phys. **56**, 104 (2006).
[32] F. Gelis and J. Jalilian-Marian, Phys. Rev. D **66**, 094014 (2002);
J. Jalilian-Marian, Nucl. Phys. A **739**, 319 (2004);
F. Gelis and J. Jalilian-Marian, Phys. Rev. D **76**, 074015 (2007).
[33] F. Dominguez, J-W Qiu, B-W Xiao and F. Yuan, Phys. Rev. D **85**, 045003 (2012).
[34] D. Zaslavsky, arXiv:1409.8259 [hep-ph].
[35] A.B. Zamolodchikov, B.Z. Kopeliovich and L.I. Lapidus, Sov. Phys. JETP Lett. **33**, 595 (1981).
[36] G. Bertsch, S.J. Brodsky, A.S. Goldhaber and J.F. Gunion, Phys. Rev. Lett. **47**, 297 (1981).
[37] S.J. Brodsky and A. Mueller, Phys. Lett. B **206**, 685 (1988).
[38] E. Iancu, K. Itakura, S. Munier, Phys. Lett. B **590**, 199 (2004).
[39] D. Kharzeev, Y.V. Kovchegov and K. Tuchin, Phys. Lett. B **599**, 23 (2004).
[40] A. Dumitru, A. Hayashigaki and J. Jalilian-Marian, Nucl. Phys. A **765**, 464 (2006).
[41] V. P. Goncalves, M. S. Kugeratski, M. V. T. Machado and F. S. Navarra, Phys. Lett. B **643**, 273 (2006).
[42] D. Boer, A. Utermann, E. Wessels, Phys. Rev. D **77**, 054014 (2008).
[43] J. T. de Santana Amaral, M. B. Gay Ducati, M. A. Betemps, and G. Soyez, Phys. Rev. D **76**, 094018 (2007);
E. A. F. Basso, M. B. Gay Ducati and E. G. de Oliveira, Phys. Rev. D **87**, 074023 (2013).
[44] G. Soyez, Phys. Lett. B **655**, 32 (2007).
[45] J. Bartels, K. Golec-Biernat, and H. Kowalski, Phys. Rev. D **66**, 014001 (2002).
[46] H. Kowalski and D. Teaney, Phys. Rev. D **68**, 114005 (2003).
[47] H. Kowalski, L. Motyka and G. Watt, Phys. Rev. D **74**, 074016 (2006);
G. Watt and H. Kowalski, Phys. Rev. D **78**, 014016 (2008).
[48] A. H. Rezaeian, M. Siddikov, M. Van de Klundert and R. Venugopalan, Phys. Rev. D **87**, 034002 (2013).
[49] A. Rezaeian and I. Schmidt, Phys. Rev. D **88**, 074016 (2013).
[50] F. D. Aaron *et al.* [H1 and ZEUS Collaborations], JHEP **1001**, 109 (2010);
H. Abramowicz *et al.* [H1 and ZEUS Collaborations], Eur. Phys. J. C **73**, no. 2, 2311 (2013).
[51] V.N. Gribov and L.N. Lipatov, Sov. J. Nucl. Phys. **15**, 438 (1972);
G. Altarelli and G. Parisi, Nucl. Phys. B **126**, 298 (1977);
Yu. L. Dokshitzer, Sov. Phys. JETP **46**, 641 (1977).
[52] G. Aad *et al.* [ATLAS Collaboration] JHEP **12**, 060 (2010).
[53] S. Chatrchyan *et al.* [CMS Collaboration] JHEP **10**, 132 (2011).
[54] S. Chatrchyan *et al.* [CMS Collaboration] Phys. Rev. Lett. **112**, 191802 (2014).
[55] G. Aad *et al.* (ATLAS Collaboration), JHEP **1406**, 112 (2014).
[56] G. Aad *et al.* (ATLAS Collaboration), Phys. Lett. B **725** 223 (2013).
[57] V. Khachatryan *et al.* (CMS Collaboration), Eur. Phys. J. **75**, 147 (2015).
[58] V. Abazov *et al.* (D0 Collaboration), Phys. Rev. D **76**, 012003 (2007).
[59] S. Chatrchyan *et al.* [CMS Collaboration], Phys. Rev. D **85**, 032002 (2012).
[60] V. Abazov *et al.* (D0 Collaboration), Phys. Rev. Lett. **100**, 102002 (2008).
[61] H. L. Lai, M. Guzzi, J. Huston, Z. Li, P. M. Nadolsky, J. Pumplin and C.-P. Yuan, Phys. Rev. D **82**, 074024 (2010).
[62] B. A. Kniehl, G. Kramer and B. Potter, Nucl. Phys. B **582**, 514 (2000).